PAPER • OPEN ACCESS

Overview of fast particle experiments in the first MAST Upgrade experimental campaigns

View the article online for updates and enhancements.

Overview of fast particle experiments in the first MAST Upgrade experimental campaigns

J.F. Rivero-Rodríguez[1,*] ⓘ, **K.G. McClements**[1] ⓘ, **M. Fitzgerald**[1], **S.E. Sharapov**[1] ⓘ, **M. Cecconello**[2,3] ⓘ, **N.A. Crocker**[4] ⓘ, **I. Dolby**[2], **M. Dreval**[5] ⓘ, **N. Fil**[1], **J. Galdón-Quiroga**[6] ⓘ, **M. García-Muñoz**[6] ⓘ, **S. Blackmore**[1], **W. Heidbrink**[7] ⓘ, **S. Henderson**[1] ⓘ, **A. Jackson**[1,2], **A. Kappatou**[8] ⓘ, **D. Keeling**[1], **D. Liu**[9], **Y.Q. Liu**[9] ⓘ, **C. Michael**[4], **H.J.C. Oliver**[1] ⓘ, **P. Ollus**[10] ⓘ, **E. Parr**[1], **G. Prechel**[7], **T. Rhodes**[4], **D. Ryan**[1] ⓘ, **P. Shi**[1], **M. Vallar**[11] ⓘ, **L. Velarde**[12], **T. Williams**[1,13], **H. Wong**[4] ⓘ, **the EUROfusion Tokamak Exploitation Team**[a] **and the MAST-U Team**[b]

[1] United Kingdom Atomic Energy Authority, Culham Campus, Abingdon, Oxon OX14 3DB, United Kingdom of Great Britain and Northern Ireland

[2] Department of Physics, Durham University, Durham DH1 3LE, United Kingdom of Great Britain and Northern Ireland

[3] Department of Physics and Astronomy, Uppsala University, Uppsala SE-751 05, Sweden

[4] Physics and Astronomy Department, University of California Los Angeles, Los Angeles, CA 90098, United States of America

[5] Institute of Plasma Physics, National Science Center, Kharkov Institute of Physics and Technology, 61108 Kharkov, Ukraine

[6] Departamento de Física Atómica, Molecular y Nuclear, Universidad de Sevilla, Sevilla, Spain

[7] Department of Physics and Astronomy, University of California, Irvine, Irvine, CA 92697, United States of America

[8] Max-Planck-Institut für Plasmaphysik, Boltzmannstr. 2, 85748 Garching, Germany

[9] General Atomics, PO Box 85608, San Diego, CA 92186-5608, United States of America

[10] Department of Applied Physics, Aalto University, PO Box 11100, 00076 AALTO, Finland

[11] Ecole Polytechnique Fédérale de Lausanne (EPFL), Swiss Plasma Center (SPC), CH-1015 Lausanne, Switzerland

[12] Departamento de Ingeniería Energética, Universidad de Sevilla, Sevilla, Spain

[13] Department of Physics and Astronomy, University of Exeter, Stocker Road, Exeter, United Kingdom of Great Britain and Northern Ireland

E-mail: juan.rivero-rodriguez@ukaea.uk

CrossMark

Abstract

MAST-U is equipped with on-axis and off-axis neutral beam injectors (NBI), and these external sources of super-Alfvénic deuterium fast-ions provide opportunities for studying a wide range of

[a] See Joffrin *et al* 2024 (https://doi.org/10.1088/1741-4326/ad2be4) for the EUROfusion Tokamak Exploitation Team.
[b] See the author list of 'Overview of physics results from MAST Upgrade towards core-pedestal-exhaust integration' by J. Harrison *et al* to be published in *Nuclear Fusion Special Issue: Overview and Summary Papers from the 29th Fusion Energy Conference (London, UK, 16–21 October 2023).*
[*] Author to whom any correspondence should be addressed.

phenomena relevant to the physics of alpha-particles in burning plasmas. The MeV range D-D fusion product ions are also produced but are not confined. Simulations with the ASCOT code show that up to 20% of fast ions produced by NBI can be lost due to charge exchange (CX) with edge neutrals. Dedicated experiments employing low field side (LFS) gas fuelling show a significant drop in the measured neutron fluxes resulting from beam-plasma reactions, providing additional evidence of CX-induced fast-ion losses, similar to the ASCOT findings. Clear evidence of fast-ion redistribution and loss due to sawteeth (ST), fishbones (FB), long-lived modes (LLM), Toroidal Alfvén Eigenmodes (TAE), Edge Localised Modes (ELM) and neoclassical tearing modes (NTM) has been found in measurements with a Neutron Camera (NCU), a scintillator-based Fast-Ion Loss Detector (FILD), a Solid-State Neutral Particle Analyser (SSNPA) and a Fast-Ion Deuterium-α (FIDA) spectrometer. Unprecedented FILD measurements in the range of 1–2 MHz indicate that fast-ion losses can be also induced by the beam ion cyclotron resonance interaction with compressional or global Alfvén eigenmodes (CAEs or GAEs). These results show the wide variety of scenarios and the unique conditions in which fast ions can be studied in MAST-U, under conditions that are relevant for future devices like STEP or ITER.

(Some figures may appear in colour only in the online journal)

1. Introduction

The Mega Amp Spherical Tokamak (MAST) has undergone a major upgrade (MAST-U) that enables higher plasma performance, state-of-the-art diagnostics and unique divertor capabilities [1]. MAST-U, with typical geometry major radius $R_0 = 0.7$ m, and minor radius $a = 0.5$ m, has a similar cross-section to other medium size conventional tokamaks, such as ASDEX Upgrade [2], and is one of the two largest spherical tokamaks worldwide, together with NSTX-U [3], enabling cross-machine analysis. The first and second MAST-U experimental campaigns achieved maximum toroidal field $B_0 = 0.65$ T at the magnetic axis and plasma current $I_\mathrm{p} = 1$ MA, and provided experimental data for a wide variety of plasma conditions [4], contributing to the understanding of the super-X divertor [5] or the development of high-beta long-pulse scenarios [6]. Results from the first experiments dedicated to fast particle physics in MAST-U are presented in this paper.

One of the main objectives of MAST-U is to study fast-ion physics and their interaction with magneto-hydro dynamic (MHD) instabilities. MAST-U is currently equipped with two neutral beam injectors (NBI) as the main source of external heating and fast ions, providing a total maximum power of $P_\mathrm{NBI} = 5$ MW. In spherical tokamaks like MAST-U, plasma ion densities (n_i) in the order of those in conventional tokamaks can be achieved with lower magnetic fields, resulting in lower Alfvén speeds ($v_\mathrm{A} = \frac{B}{\sqrt{\mu_0 n_\mathrm{i} m_\mathrm{i}}}$), where m_i is the ion mass and μ_0 is free space permeability. On the other hand, the NBI energy is similar to those in conventional tokamaks, so the fast-ion velocities (v_b) can be close to or above the Alfvén speed (super-Alfvénic) and can therefore come in the resonance with Alfvén waves during their slowing-down and excite a wide range of Alfvénic instabilities. These are conditions that are relevant for, e.g. ITER, where the NBI will provide

such an anisotropic super-Alfvénic fast-ion distribution, driving together with isotropic fusion-born alpha-particles similar Alfvénic instabilities that can affect the heating and current drive available to achieve burning plasmas. Thus, understanding the fast-ion dynamics in MAST-U is not only relevant for spherical tokamaks but also for future conventional tokamaks with burning plasmas, as the MAST-U beam ions mimic some of the conditions of burning plasmas. The interplay between fast ions and MHD instabilities, and the resulting fast-ion redistribution and loss, was explored in MAST [7], where the correlation between steep fast-ion pressure gradients and the drive of MHD instabilities was demonstrated experimentally [8, 9]. MAST-U provides a more versatile fast-ion distribution, as it offers on-axis and off-axis NBI with the aim of providing broader plasma heating and the non-inductive current drive profiles, minimising the radial gradient of the fast ion pressure and decreasing the drive of MHD instabilities and fast-ion losses. An improved set of fast-ion diagnostics makes it possible to study their redistribution and loss with good spatial and temporal resolution. The fast-ion diagnostics in MAST-U include a fast-ion deuterium-α (FIDA) spectrometer [10], measuring Doppler-shifted Balmer-α emission due to charge exchange between fast ions and neutrals; a solid-state neutral particle analyser (SSNPA) [11] detecting fast neutrals from charge exchange reactions; a scintillator-based fast ion loss detector (FILD) [12], providing the velocity space distribution of lost fast ions and the frequencies of modes correlated with these losses; an upgraded neutron camera (NCU) [13] measuring neutron flux mainly resulting from beam-thermal fusion reactions along 6 lines of sight on the equatorial plane; and a fission chamber (FC) [14], measuring the total neutron flux. For measurements of fast ion-driven instabilities, the MAST-U is equipped with the outboard Mirnov coil array for high frequency acquisition (OMAHA)

[15], providing $\mathrm{d}(\delta B)/\mathrm{d}t$ measurements that makes it possible to detect magnetic perturbations in the plasma; beam emission spectroscopy (BES) [16] and Doppler backscattering (DBS) [17], which provide *in situ* measurements of fluctuations and also spatial information on mode structure. A motional Stark effect (MSE) diagnostic [18] measures the equilibrium magnetic field pitch as function of radius, which is also an important tool for studying the co-evolution of fast-ions and thermal plasma.

This paper is structured as follows: The fast-ion distribution and losses produced by on-axis and off-axis beams are discussed in section 2. The instabilities driven by fast ions are described in section 3 and the fast-ion transport and losses induced by thermal plasma-driven instabilities is covered in section 4. Finally, the results are discussed in section 5.

2. On and off-axis neutral beam injection

External heating and fast ions in MAST-U are provided by two neutral beam injectors (NBI) directed tangential to the plasma and co-current, each providing up to 2.5 MW of external heating, and deuterium fast ions with energies up to 75 keV. While both sources were on-axis in MAST, the south-west NBI has been later raised 65 cm above the vacuum vessel equatorial plane for MAST-U. Thus, on-axis (south) and off-axis (south-west) beams produce a peaked and a hollow fast-ion profile, respectively, as demonstrated experimentally by the count rates (CR) measured with the NCU in figure 1. Combined, the two beams produce a relatively flat fast-ion profile that reduces the radial gradient of the fast ion distribution in comparison to the previous MAST settings. This reduces the drive of MHD instabilities, as observed in MAST experiments [9]. Indeed, MAST-U plasmas heated with the on-axis NBI are more likely to develop MHD instabilities that are detrimental to the thermal plasma and the fast-ion confinement, such as fishbones (FBs), sawteeth (ST), long-lived modes (LLMs) or neoclassical tearing modes (NTMs), than plasmas heated with both beams, even if the injected power is higher with two beams. This has made it possible to achieve higher performance plasmas with substantial heating and minimal fast ion losses.

In the first campaign, the neutron rate produced by off-axis NBI was 10 times smaller than that provided by on-axis NBI despite the injected power of the two beams being comparable [19]. This suggested low confinement of off-axis fast-ions. The low plasma elongation used during the first campaign ($\kappa < 2$) partly explains this result, as it caused the off-axis NBI to deposit fast ions closer to the last closed flux surface, diminishing their confinement. However, later shots with $\kappa = 2.13$ still show a neutron rate 4.2 times higher with on-axis than off-axis injection. Since approximately 90% of the total neutron emission comes from beam-thermal fusion reactions, the on-axis beam is expected to produce more neutrons even without losses, as it deposits ions closer to the plasma core where the temperature and density are higher.

The neutron rate and passive FIDA measurements are generally better matched by the ASCOT fast-ion orbit following code when the modelling accounts for charge exchange (CX) losses [20], as observed in figure 2. The simulations are based on a high field side fuelled plasma, and the edge neutral density was estimated based on midplane D-α and Thomson scattering measurements and assumed to be poloidally uniform. Due to Shafranov shift, orbit drifts and major-radius-dependent gyroradii, MAST-U has fast-ion orbits that are weighted towards the outer radius midplane, where the neutral density was calculated. Thus, poloidal uniformity is deemed acceptable. The simulations indicated that up to 20% of NBI fast ions can be lost due to charge exchange (CX) with edge neutrals. Thus, the effect of CX losses in edge fast-ion confinement was investigated experimentally in MAST-U shot #46735, where the fuelling was switched from high field side (HFS) valves to low field side (LFS) valves at $t = 0.30$ s, thus increasing the LFS edge neutral density to enhance edge CX losses. Figure 3 shows that the edge passive FIDA emission, which is correlated with both the fast-ion density and the neutral density, transiently drops after the fuelling change, indicating a drop in edge fast-ion confinement, before it partially recovers as the inflowing neutrals diffuse around the plasma. The neutron rate decreases even before the main chamber neutral pressure at the LFS increases and earlier than the core electron temperature decreases. The drop in the measured neutron rate is larger than that estimated by TRANSP after the fuelling switch. Since TRANSP does not directly account for the fuelling switch, the drop in the modelled neutron rate is an estimate of the intrinsic drop due to changes in electron temperature and density. Thus, the difference between measured and estimated rates after the fuelling switch indicates an increase in CX losses with LFS fuelling. Moreover, since the TRANSP simulation is based on measured electron temperature, the drop in temperature and its effect on the neutron rate may be indirectly caused by CX losses. The observations immediately after the change in fuelling location reveal patterns that fit an increase of edge CX losses caused by the increase of LFS edge neutral density. However, changes in the electron density and plasma rotation can be playing a role on the subsequent neutron rate and core electron temperature decrease, which will be addressed further [21].

The difference between on-axis and off-axis beam deposition has a significant effect on fast-ion prompt losses [22], defined as fast ions that lose confinement in less than an orbital time. The prompt losses from the on-axis beam detected by FILD produce a single spot localised in pitch angle, while the prompt losses from the off-axis beam produce a set of spots distributed in a wide range of pitch angles, as observed in figure 4. In the experiment, the injection energy of each beam is chosen to improve its reliability while maximising the injected power. Nonetheless, this has only a minor effect on the beam deposition, while the plasma density and the beam geometry are the dominant parameters. Since the MAST-U beams are non-steerable, the FILD data provides a good estimate of the beams' injected pitch angles. Figure 5 shows the prompt
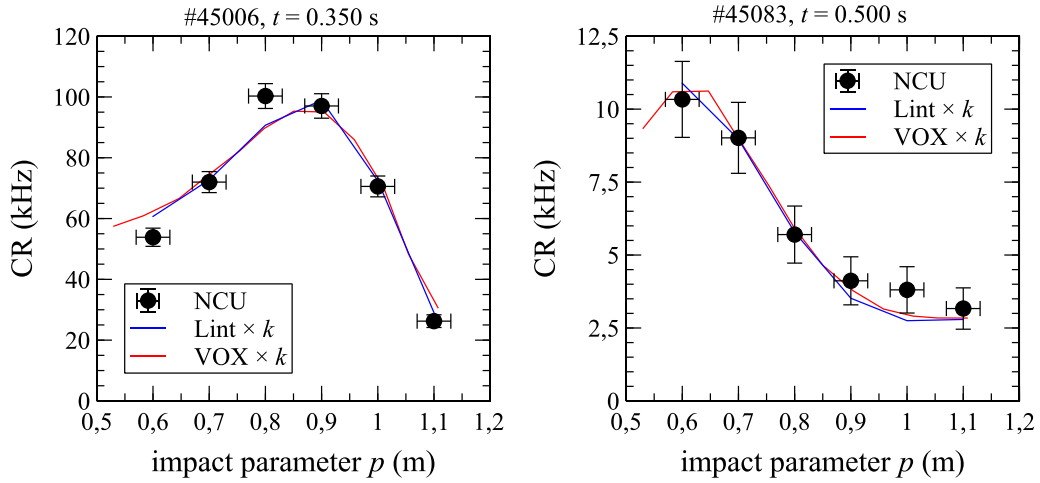
Figure 1. Comparison between neutron emission produced by the on-axis (left) and off-axis (right) beams measured by NCU (black solid circles) and predicted by TRANSP using simple line of sight integrals (Lint, blue line) and the full 3D field of view geometry (VOXels, red line). A scaling factor $k = 0.4$ has been applied to the Lint and VOXel count rate values to normalise them to the NCU measurements. Reproduced from [19]. CC BY 4.0.
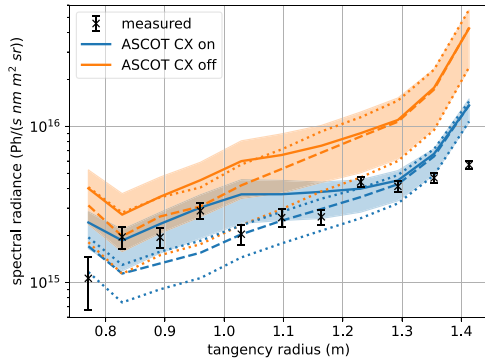

Figure 2. ASCOT5-FIDASIM-simulated and bremsstrahlung-corrected measured passive FIDA signals (logarithmic scale) in shot #45091 at 0.35 s as functions of the tangency radii of the FIDA channels. Reproduced from [20]. CC BY 4.0.

losses modelled with ASCOT from the on-axis and the off-axis beam. The on-axis fast ions follow trapped orbits while the off-axis beam prompt losses are passing. Due to the large difference in toroidal frequency between passing and trapped orbits and the deeper ionization profile of the off-axis beam, the off-axis beam produces an almost axi-symmetrical prompt loss distribution along the LFS midplane, whereas the prompt losses from the on-axis beam are toroidally localised between $0°$ and $100°$.

3. Fast-ion driven instabilities

3.1. Global and compressional Alfvén eigenmodes

In MAST-U, where $v_b/v_A \approx 2$, energetic particle-driven modes in the range of the 1–2 MHz have been detected with the OMAHA coils. This is 0.2–0.5 times the cyclotron frequency of deuterium at the magnetic axis ($f_{ci} \approx 4.1$ MHz).
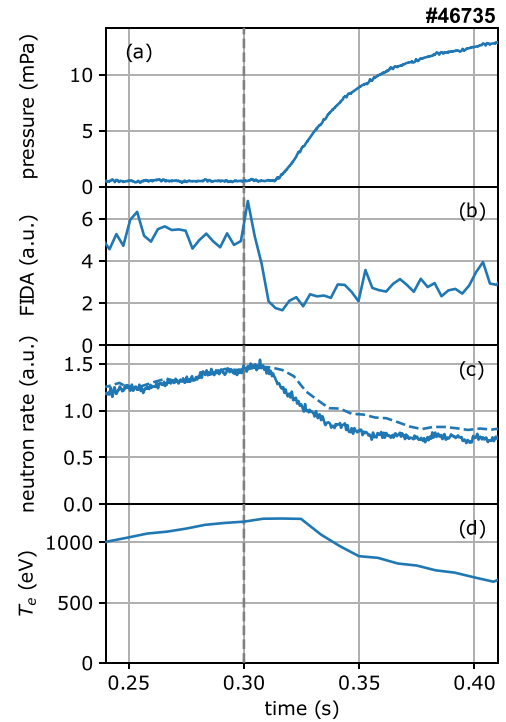

Figure 3. From top to bottom, neutral pressure at the LFS, edge passive FIDA emission, neutron rate measured by the fission chamber (solid line) and estimated by TRANSP (dashed line), and core electron temperature of MAST-U shot #46735.

The modes are in the frequency range where Compressional Alfvén Eigenmodes (CAEs) and Global Alfvén Eigenmodes (GAEs) were identified in MAST [23, 24] and NSTX [25, 26]. The modes are observed at all values of plasma current, $I_p = [450, 750]$ kA, and magnetic field, $B_t^{axis} = [0.45, 0.65]$ T. They are more frequently observed in on-axis and two-beam heated plasmas, indicating stronger drive from the on-axis
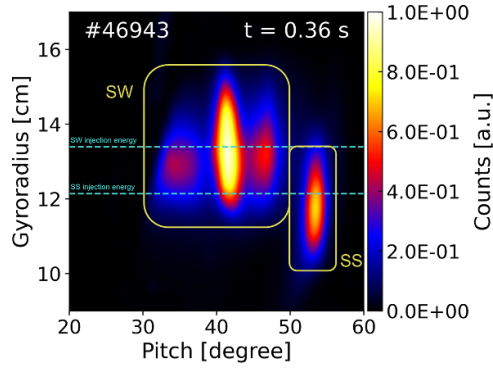
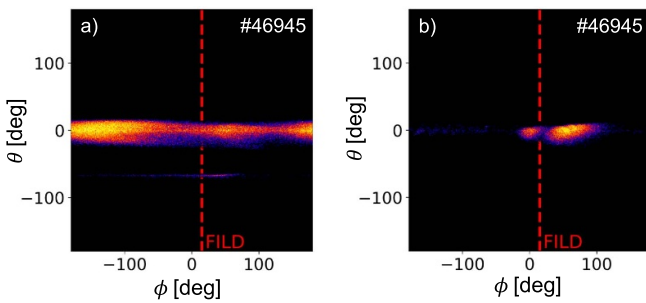**Figure 4.** Velocity-space of the losses measured by FILD corresponding to on-axis (SS) and off-axis (SW) beam.

Figure 5. Prompt-loss distribution in toroidal and poloidal angles of the off-axis (*a*) and on-axis (*b*) beam modelled with ASCOT. Reproduced from [22]. © The Author(s). Published by IOP Publishing Ltd. CC BY 4.0.

beam. Moreover, NCU data show that, in sawteething plasmas, the modes are interrupted by the sawtooth crashes, when the fast ion profile flattens, and they only reappear when the fast ion profile recovers, showing the fast-ion driven nature of these modes [27].

FILD measurements have revealed coherent fast-ion losses matching the frequency of high frequency Alfvén instabilities [27], showing that they can induce fast-ion losses and can have an adverse impact on the fast-ion confinement. A polarization analysis of the OMAHA coils suggests that the fast-ion losses are correlated with compressional rather than shear waves. However, this inference relies on the edge polarization of the wave, which does not always match the internal polarization of the modes. The Doppler backscattering spectroscopy (DBS) diagnostic has been used to localise the modes that caused fast-ion losses, as shown in figure 6. It can be observed that the modes that do not cause fast-ion losses are more core localised, extending up to normalised radial distance $\psi_n^{1/2} = 0.7$, likely causing fast-ion redistribution without losses, whereas the modes that produce fast-ion losses extend up to $\psi_n^{1/2} = 0.9$, closer to the edge. Due to hardware limitations, the redistribution of fast ions near the plasma core is not characterised, but it remains a key point to investigate in future analyses and experiments. Mode number analysis estimates toroidal mode numbers with absolute values in the

range of 4–10. The analysis shows the coexistence of modes that have phase velocities in the opposite direction of the beam and the plasma current (counter-current), whose toroidal mode number decreases with frequency, and modes that have phase velocities in the direction of the beam and the plasma current (co-current), whose toroidal mode number increases with frequency. This suggests that the modes can be driven unstable by both normal and anomalous Doppler-shifted ion-cyclotron resonance with the fast-ions, although CAEs driven by the Landau–Cherenkov resonance have been reported before [7] and cannot be ruled out. The linear stability code MISHKA3 [28] has been employed to model the MAST-U plasmas in which the losses are observed. The results successfully reproduce $n = 6$ compressional waves in the range of 1-3 MHz with eigenfunctions peaking around $r \approx 0.35$ m, and significant structure up to the mid-radius and propagating counter-current. This suggests that the modes responsible for the fast-ion losses are CAEs.

The spectrum covers a wide range of frequencies with a clear frequency splitting on three different scales: 300 kHz, 150 kHz and 25 kHz. If the modes were CAEs, the splitting can be theoretically explained by the frequency separation due to different values of radial number, *s*, poloidal mode number, *m*, and toroidal mode number, *n*, respectively [24, 29]. The fast-ion losses are very sensitive to this frequency splitting. This indicates a resonant transport of the fast-ion losses, as the losses are very sensitive to the mode structure.

3.2. Ion cyclotron emission

Bursts of 1st harmonic ion cyclotron emission (ICE) core density perturbations ($\widetilde{n}_e$) with $k_\perp \rho_s \geqslant 1$ (ρ_s being the ion sound Larmor radius) have been observed in ohmic plasmas (without NBI heating) using a Doppler backscattering (DBS) diagnostic provided by University of California Los Angeles [30]. The ohmic ICE stability shows a dependence on the plasma *q*, since it is only driven unstable at $B_T/I_p \leqslant 0.9$ T/MA. ICE is commonly observed to be excited by energetic ions and is anticipated to be useful in diagnosing features of the fast-ion distribution [31, 32]. The fact that ICE is observed in ohmic discharges, where the fast ion content is expected to be low, poses a challenge to this theory. Possible explanations for this ohmic ICE include cyclotron drift wave excitation and the transient production of fast-ions in reconnection events.

3.3. Toroidicity-induced Alfvén eigenmodes

Magnetic perturbations at the beginning of MAST-U shots are often observed typically around 85 kHz, chirping down in frequency by about 20 kHz, then stabilising and reappearing in a bursting cycle [33]. The modes have been identified as Toroidally-induced Alfvén Eigenmodes (TAEs) using the stability code MISHKA. The TAEs are observed to move in the direction of the beam and the plasma current (co-current),
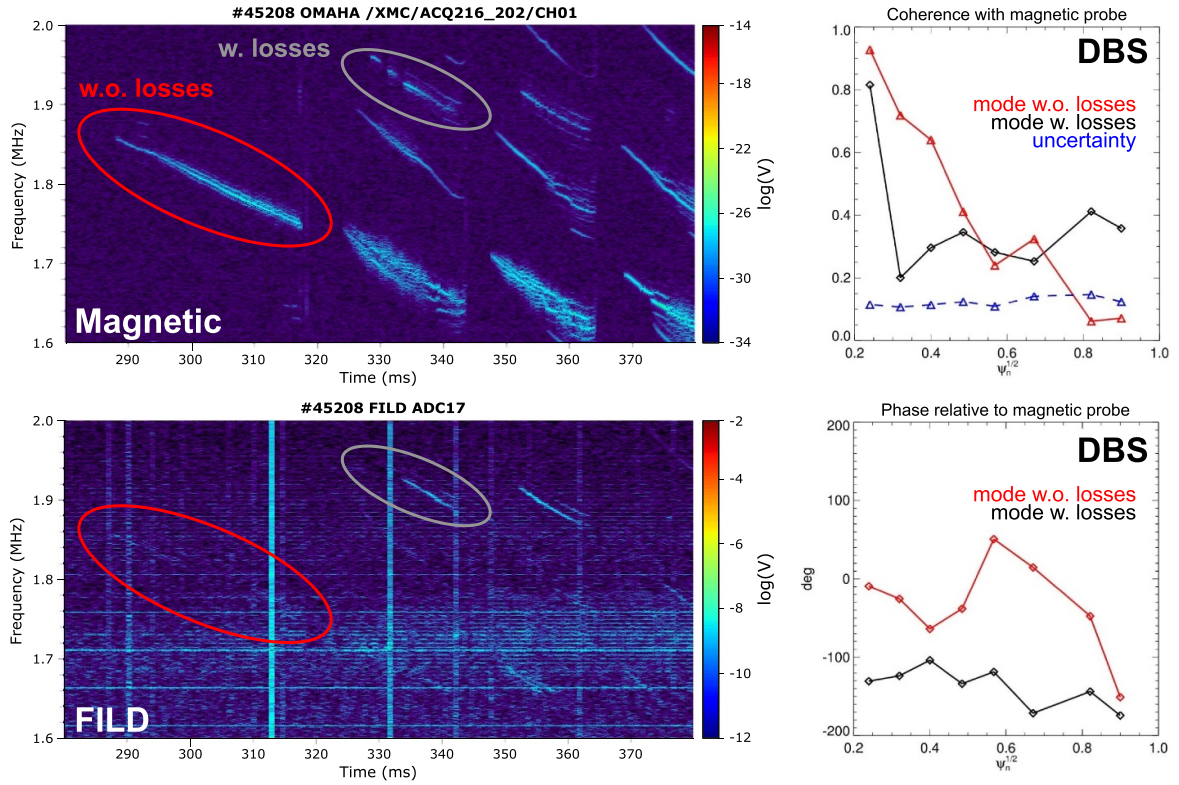
Figure 6. MAST-U shot #45208, a 750 kA H-mode plasma. (left) Spectrograms of a Mirnov coil (top) and FILD (bottom). (right) DBS coherence (top) and phase (bottom) relative to magnetic probe of modes seen and not seen by FILD.

as expected, with toroidal mode numbers between $n = 1$ and $n = 4$.

TAEs can be detected as density fluctuations in BES data, and are correlated with changes in FIDA emission that indicate fast ion transport. However, the chirping and bursting of the TAEs reveals only a slight redistribution of fast ions from the outboard to the inboard side in NCU profiles [19]. This suggests that the TAEs cause sufficient fast-ion redistribution to generate the chirping and bursting cycle of the modes, but do not affect the fast-ion confinement severely. This is confirmed by FILD measurements, as observed in figure 7, which shows that the total fast ion losses are barely affected by the bursting TAEs [34]. FILD only detects losses coherent with the TAE frequency from the off-axis beam, but the modulated losses disappear in less than a slowing down time after the off-axis beam is switched off, indicating that FILD is detecting prompt losses from the off-axis beam modulated with the TAEs. This contrasts with NSTX-U observations, that shows fast-ion and thermal plasma losses induced by TAE avalanche, a non-linear event resulting from wave-wave coupling and wave-particle resonances overlap [35, 36]. The results from NSTX-U suggest that such a non-linear interaction between TAEs may only occur with higher beam power and different beam geometry than in MAST-U and motivates non-linear analysis of the modes in future work.

MISHKA modelling and BES analysis shows that the TAEs are localised near the edge. This explains the relatively moderate effect of TAEs in the NCU neutron rate (it is more

sensitive to core distributions) and the modulation of off-axis prompt losses. Modes in lower frequency range whose Alfvénic frequency scale with ion density are detected but not identified yet.

3.4. Fishbones and long-lived modes

Fishbones (FB) and long-lived modes (LLM) are driven unstable in MAST-U L-mode plasmas with on-axis heating, sufficiently low plasma densities, and q_{min} close to 1, as illustrated in figure 8. In such conditions, linear stability analysis using the MARS-F MHD code [37] shows an $n = 1$ internal kink mode unstable when $q_{min} < 1.1$ that is responsible for the FB and the LLM. However, FBs and LLMs in MAST-U are scarcer and weaker than in MAST. This is mainly caused by the lower amount of on-axis power available, reducing the core fast-ion densities available to drive them unstable. FBs are responsible for core fast-ion redistribution and loss: as the FB grows, the neutron profile begins to change, developing a hollow-profile indicating a loss of core fast ions. After the FB, the neutron rate profile starts to recover and becomes core-peaked again [19]. This drop in core fast ions during the FB is confirmed by SSNPA and FIDA [11], while the FB-induced losses detected by FILD are observed to follow trapped orbits whose inner leg sits near the plasma core. This may indicate losses caused by pitch-angle scattering.

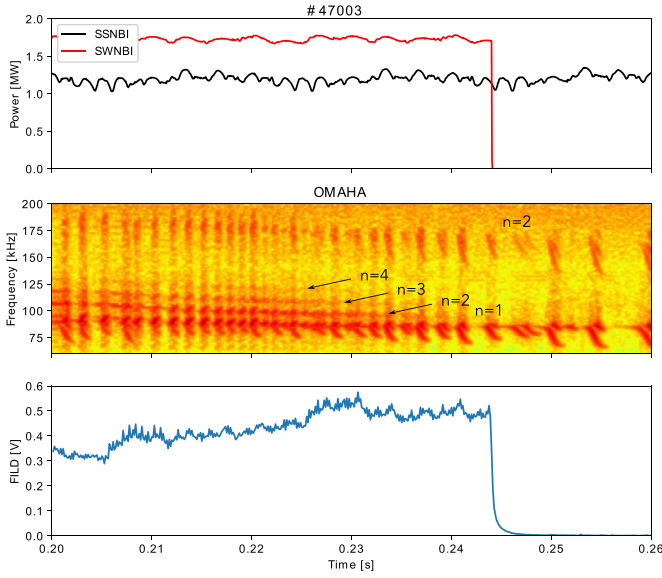BES and MSE analyses show that the drop in core fast ions induced by the FBs produces rapid changes in equilibrium

Figure 7. Chirping TAEs in MAST-U shot #47003. From top to bottom, NBI injected power, spectrogram of the magnetic perturbation from OMAHA coils and fast-ion losses from FILD [34].

Figure 8. MAST-U shot #45132, a 750 kA L-mode plasma. From top to bottom, line integrated density, q_0, neutron rate from FC, fast-ion losses from FILD and magnetic perturbation from OMAHA coils [34].

conditions [38]. The magnetic axis moves outward before the FB as the fast-ion pressure builds up and then rapidly inward caused by changes in Shafranov shift due to the loss of core fast-ion pressure during the FB. This analysis is in line with NCU observations, that show a post-FB peak closer to the HFS, indicating the inward shift of the magnetic axis. The results emphasize the importance of considering equilibrium changes in the models to predict FB growth and chirping rates in future fusion devices. LLM commonly appear after the FB phase, also revealing fast-ion redistribution and an inward shift of the magnetic axis in the NCU measurements but no losses in the FILD data.

4. Fast-ion loss and redistribution

4.1. Sawteeth

Sawteeth are mostly observed in L-mode plasmas with on-axis beam when $q_{\min} < 1$, as shown in figure 8. While the drops in the NCU neutron rate associated with sawteeth imply that up to 40%–50% of the total neutron yield is lost during a sawtooth [19], the FILD signal correlated with the sawteeth indicate more moderate fast-ion losses. The losses observed during a sawtooth are only 25% of the losses observed during a FB, and often sawtooth losses are not even detected. This suggests that sawteeth are responsible for a large redistribution, rather than loss, of core fast ions, which combined with the typical reductions in core temperature during a sawtooth, causes the drop in the neutron rate, as observed in JET using a 2D neutron camera [39]. Sawteeth-induced losses are higher in low current plasmas, as the overall confinement is lower and the redistribution induced by sawteeth lead to fast-ion losses. Nonetheless, to give a more quantitative assessment of the losses, an absolute calibration of FILD will be required. As observed in figure 8,
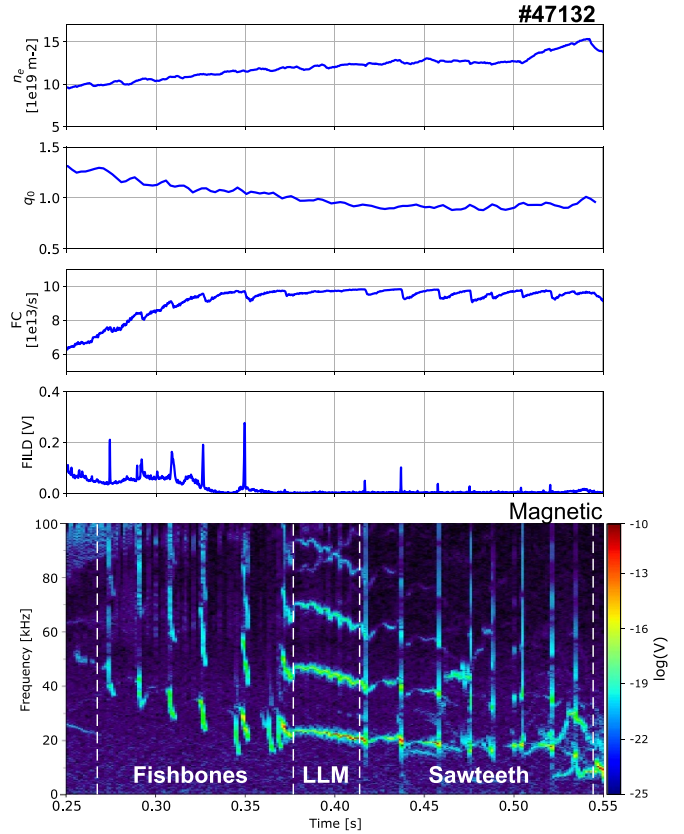
sawtooth crashes are always preceded by LLMs, suggesting a synergy between the modes that may lead to an increase in the fast-ion losses, similarly to that observed in HL-2A [40].

4.2. Neoclassical tearing modes

Neoclassical tearing modes (NTMs) are ubiquitous in MAST-U beam-heated plasmas with $I_{\text{p}} = 750$ kA [4], causing the largest fast-ion losses. The most common type of NTM is identified as having $(m, n) = (2, 1)$ magnetic islands, located at the $q = 2$ rational flux surface, at about the frequency of the local plasma toroidal rotation (8–10 kHz). During the NTM phase, both the fission chamber and NCU show a decrease in the neutron rate, below that estimated by TRANSP/NUBEAM simulations, as observed in figure 9, indicating a fast ion transport induced by the NTM that is not captured by the code. The characterisation of the NTM-induced transport will require full orbit simulations with Monte-Carlo codes like ASCOT. Eulerian Video Magnification (EVM) [41] has been applied to FILD data with the aim of enhancing variations in the fast-ion loss velocity space at the frequency of the NTM. The analysis revealed fast-ion losses that sweep up and down in pitch angle at the NTM frequency, illustrating the deflection caused by the NTM on the fast-ion orbits as it rotates with the plasma.
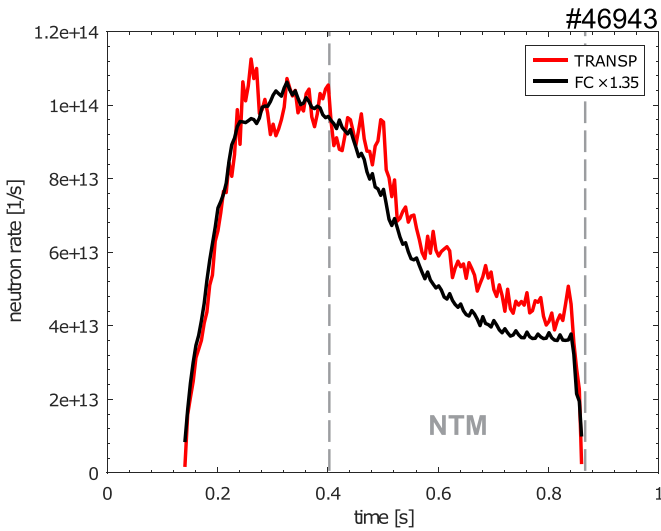
Figure 9. Comparison between neutron rate measured by the FC and estimated by TRANSP. A scaling factor of 1.35 has been applied to the FC data to match the TRANSP results at the beginning of the discharge.

4.3. Edge localised modes

Spikes of fast-ion losses correlated with edge localised modes (ELMs) are observed in MAST-U [42, 43]. They are identified as type-III ELMs, with burst frequencies around 200 Hz. The ELM-induced losses are localised in velocity-space, as shown in figures 10(*a*) and (*b*). The fact that type-III ELMs induce the loss of specific fast-ion orbits suggests a resonant interaction between the fast ion orbits and the perturbation. The FILD signal is consistent with the SSNPA passive signal, that is assumed to originate at the plasma edge, where CX reactions with thermal (passive) neutrals are more numerous. SSNPA measures reductions of the most energetic ions and pitch angles above 69° correlated with the ELMs, as observed in figure 10(*c*). This indicates loss of passing fast ions, in line with FILD data. Passive FIDA also indicates fast-ion losses from the off-axis beam correlated with type-III ELMs [44]. ELMs barely affect the neutron rate from the fission chamber or NCU, showing once more that edge fast ions have only a moderate effect on the neutron flux.

4.4. Internal reconnection events

Ion acceleration during reconnection events was reported in MAST [45]. In MAST-U, spikes in the SSNPA signal correlated with internal reconnection events (IRE) have been observed [46, 47]. The SSNPA consists of 3 arrays of channels that are covered by progressively thicker tungsten foils to block different energies, giving information on the fast-ion energy distribution. The spikes correlated with the IRE have larger relative amplitudes between the arrays than that expected for the maximum NBI energy, indicating the detection of fast-ions with energies above the NBI injection energy. FILD also detects losses correlated with the IRE above the injection energy with pitch angles above 70°, meaning that the accelerated fast ions follow deeply trapped orbits. This is in
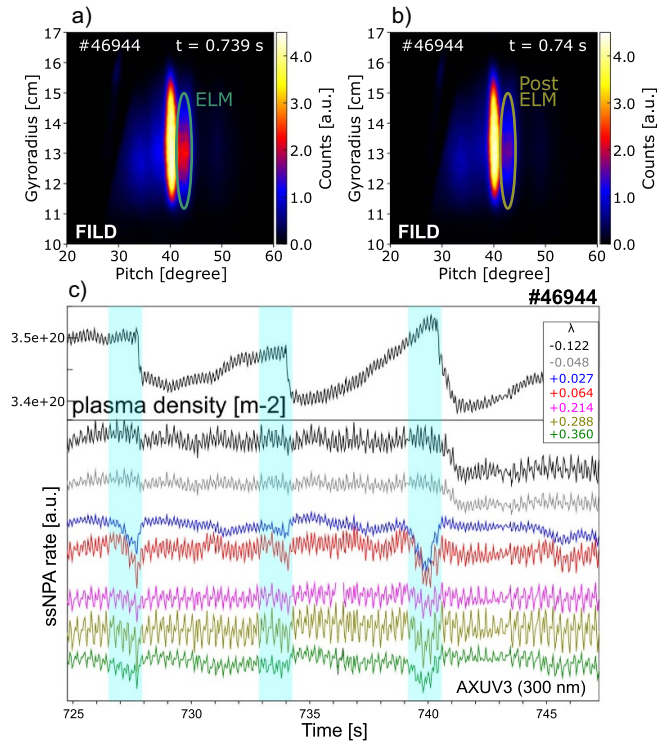

Figure 10. FILD losses during (*a*) and after (*b*) a type-III ELM. The velocity-space of the losses induced by type-III ELMs are circled [42]. (*c*) Line integrated density and SSNPA passive signal. The ELM crashes is shaded in blue [43].

line with SSNPA data, which predominantly measures trapped particles. Spikes in the soft x-ray data also strongly suggest electron acceleration during IREs. Reconnection events during the plasma ramp-down have also revealed spikes in SSNPA and FILD a few slowing down times after the NBI shuts down, showing acceleration of thermal ions.

5. Summary and conclusions

The first experimental campaigns in MAST-U have provided key information to understand the confinement of fast ions in spherical tokamaks and in conditions that mimic those of fusion products in future burning plasmas. The variety of fast-ion diagnostics in MAST-U makes it possible to consistently assess the confined and lost fast ions with unique spatial and temporal resolution, expanding the understanding on fast-ion redistribution and losses from MAST and revealing new physics relevant to spherical tokamaks and burning plasmas. The combination of on-axis and off-axis NBI has been shown to improve the heating performance, as it reduces the core-peaking of the fast-ion distributions and the pressure gradients, suppressing the drive of instabilities that are deleterious for the fast-ion confinement. The experiments have also made it possible to quantify CX-induced losses of edge fast ions in spherical tokamaks.

The unprecedented measurements of losses induced by high-frequency AEs are the most direct evidence that CAEs

and GAEs have an adverse impact on the fast-ion confinement. This is not only relevant for spherical tokamaks but also for future burning plasmas in ITER, where the NBIs will provide an anisotropic super-Alfvénic fast-ion population that can potentially drive CAEs and GAEs unstable. Thus, the fast-ion redistribution and loss associated with high-frequency AEs can affect the heating and current drive available to achieve burning plasmas. MAST-U shows that TAEs have only a minor effect on fast-ion redistribution and losses, which contrasts with the results from conventional tokamaks like AUG [48], where TAEs are a significant cause of fast-ion losses, and spherical tokamaks of comparable size like NSTX-U [35, 36], where the losses are the result of non-linear wave-wave coupling and wave-particle resonance overlap. In future work non-linear analysis will be performed to investigate this important difference in MAST-U. Ions accelerated by reconnection events provide a possible explanation of ICE detected using DBS in ohmic plasmas.

The MAST-U fast-ion diagnostics, such as SSNPA, NCU, FIDA and FILD, together with the on-going commissioning of the charged fusion product detector (CFPD), made it possible to address the fast-ion redistribution and losses due to a wide variety of instabilities. NTMs are the most deleterious modes in MAST-U, as they produce the highest losses, as measured by FILD, and they require the largest anomalous diffusion rates in TRANSP/NUBEAM to match the neutron rate measured by NCU. LLMs and FBs also degrade the fast-ion confinement, but they are infrequent in MAST-U. ELMs produce a considerable amount of edge fast-ion loss and redistribution but a negligible effect on the neutron flux. On the other hand, sawteeth cause large drops in the neutron flux but moderate losses, indicating that sawteeth are responsible for a large redistribution of core fast ions but relatively few losses.

A deleterious effect of externally applied fields, such as resonant magnetic perturbations, error fields and toroidal field ripple on the fast-ion confinement has been observed in MAST-U and will be characterised in future campaigns. MAST-U includes two rows of in-vessel saddle coils for ELM control with Resonant Magnetic Perturbations (RMPs). RMPs have been shown to affect the fast-ion confinement in, for example, ASDEX Upgrade [49, 50], DIII-D [51], KSTAR [52], MAST [53], while ASCOT modelling predicts a similar effect in ITER [54]. Current experiments are addressing the effect of RMPs on fast ions in MAST-U. Additionally, active control of TAEs excitation and suppression with RMPs have been achieved in NSTX [55] and ASDEX Upgrade [56]. Given the wide variety of AEs driven unstable in MAST-U, this device is ideal to explore AE suppression with RMPs and also their effect on high frequency AEs.

The MAST-U experimental results provide valuable information to study the behaviour of fast particles and their interaction with MHD instabilities in conditions that resemble those of future burning plasmas, where super-Alfvénic alpha particle heating will dominate. Future campaigns will study the fast-ion behaviour in higher performance plasmas with up to 2 MA of plasma current, including Alfvén and acoustic modes stability in high-beta plasmas with parameters similar to those expected in the Spherical Tokamak for Energy Production (STEP) [57]. Significant enhancements are planned in the next years, including the installation of a double beam box, that will provide up to 2.5 MW of additional off-axis heating and 2.5 MW of intermediate injection between on-axis and off-axis. The addition of extra NBI power with a versatile fast-ion distribution will provide further opportunities to study fast-ion effects, including the drive of AEs by alpha-particles in burning plasmas and mitigation techniques with off-axis beam, and it will help to increase the non-inductive current drive, which will provide key information to achieve sustained operation in future power plants.

Acknowledgments

ORCID iDs

J.F. Rivero-Rodríguez ⓘ https://orcid.org/0000-0001-5074-0267
K.G. McClements ⓘ https://orcid.org/0000-0002-5162-509X
S.E. Sharapov ⓘ https://orcid.org/0000-0001-7006-4876
M. Cecconello ⓘ https://orcid.org/0000-0002-2571-1920
N.A. Crocker ⓘ https://orcid.org/0000-0003-2379-5814
M. Dreval ⓘ https://orcid.org/0000-0003-0482-0981
J. Galdón-Quiroga ⓘ https://orcid.org/0000-0002-7415-1894
M. García-Muñoz ⓘ https://orcid.org/0000-0002-3241-502X
W. Heidbrink ⓘ https://orcid.org/0000-0002-6942-8043
S. Henderson ⓘ https://orcid.org/0000-0002-8886-1256
A. Kappatou ⓘ https://orcid.org/0000-0003-3341-1909
Y.Q. Liu ⓘ https://orcid.org/0000-0002-8192-8411
H.J.C. Oliver ⓘ https://orcid.org/0000-0002-7302-085X
P. Ollus ⓘ https://orcid.org/0000-0003-2558-1457
T. Rhodes ⓘ https://orcid.org/0000-0002-8311-4892
D. Ryan ⓘ https://orcid.org/0000-0002-7735-3598
M. Vallar ⓘ https://orcid.org/0000-0002-1792-6702
H. Wong ⓘ https://orcid.org/0000-0003-0923-9141

References

[1] Harrison J. *et al* 2024 *Plasma Phys. Control. Fusion* **66** 065019
[2] Stroth U. *et al* 2022 *Nucl. Fusion* **62** 042006
[3] Menard J.E. *et al* 2017 *Nucl. Fusion* **57** 102006
[4] Harrison J. *et al* 2024 *Nucl. Fusion* submitted
[5] Verhaegh K. *et al* 2024 *Nucl. Fusion* **63** 016014
[6] Coda S. *et al* 2024 *Nucl. Fusion* submitted
[7] Cecconello M. *et al* 2015 *Plasma Phys. Control. Fusion* **57** 014006
[8] Turnyanskiy M. *et al* 2013 *Nucl. Fusion* **53** 053016
[9] Keeling D. *et al* 2015 *Nucl. Fusion* **55** 013021
[10] Michael C.A. *et al* 2013 *Plasma Phys. Control. Fusion* **55** 095007
[11] Prechel G. *et al* 2022 *Rev. Sci. Instrum.* **93** 113517
[12] Rivero-Rodriguez J.F. *et al* 2018 *Rev. Sci. Instrum.* **89** 10I112
[13] Cecconello M. *et al* 2018 *Plasma Phys. Control. Fusion* **60** 055008
[14] Vincent C. *et al* 2022 *Rev. Sci. Instrum.* **93** 093509
[15] Hole M.J. *et al* 2009 *Rev. Sci. Instrum.* **80** 123507
[16] Field A.R. *et al* 2009 *Rev. Sci. Instrum.* **80** 073503
[17] Rhodes T.L. *et al* 2022 *Rev. Sci. Instrum.* **93** 113549
[18] Conway N.J. *et al* 2010 *Rev. Sci. Instrum.* **81** 10D738
[19] Cecconello M. *et al* 2023 *Plasma Phys. Control. Fusion* **65** 035013
[20] Ollus P. *et al* 2024 *Plasma Phys. Control. Fusion* **66** 025009
[21] Ollus P. *et al* 2024 *Nucl. Fusion* (in preparation)
[22] Velarde L. *et al* 2024 *Plasma Phys. Control. Fusion* (in preparation)
[23] Appel L.C. *et al* 2008 *Plasma Phys. Control. Fusion* **50** 115011
[24] Sharapov S.E. *et al* 2014 *Phys. Plasmas* **21** 082501
[25] Fredrickson E. *et al* 2001 *Phys. Rev. Lett.* **87** 145001
[26] Gorelenkov N.N. *et al* 2003 *Nucl. Fusion* **43** 228–33
[27] Rivero-Rodriguez J.F. *et al* 2022 *48th EPS Conf. on Plasma Physics*
[28] Mikhailovskii A.B. *et al* 1998 *Plasma Phys. Control. Fusion* **40** 1907–20
[29] Gorelenkov N.N. *et al* 2006 *Nucl. Fusion* **46** S933
[30] Crocker N.A. *et al* 2024 *Nucl. Fusion* (in preparation)
[31] McClements K.G. *et al* 2015 *Nucl. Fusion* **55** 043013
[32] Gorelenkov N.N. *et al* 2016 *New J. Phys* **10** 105010
[33] McClements K.G. *et al* 2022 *48th Plasma Physics Conf.*
[34] Rivero-Rodriguez J.F. *et al* 2023 *5th European Conf. on Plasma Diagnostics* (*Crete, Grece*, *April 2023*) (available at: ecpd2023.eventsadmin.com)
[35] Podestá M. *et al* 2012 *Nucl. Fusion* **52** 094001
[36] Zhu X. *et al* 2022 *Nucl. Fusion* **62** 016012
[37] Liu Y.Q. *et al* 2000 *Phys. Plasmas* **7** 3681
[38] Wong H. *et al* 2023 *29th IAEA Fusion Energy Conf.* (*London, United Kingdom, October 2023*) (available at: www.iaea. org/events/fec2023)
[39] Kiptily V.G. *et al* 2022 *Plasma Phys. Control. Fusion* **64** 064001
[40] Zhu X. *et al* 2023 *Nucl. Fusion* **63** 036014
[41] Wu H.Y. *et al* 2012 *ACM Trans. Graph.* **31** 1–8
[42] Velarde L. *et al* 2023 *49th EPS Conf. on Plasma Physics* (*Bordeaux, France, July 2023*) (available at: https:// eps2023.github.io/)
[43] Galdon-Quiroga J. *et al* 2023 *49th EPS Conf. on Plasma Physics* (*Bordeaux, France, July 2023*) (available at: https:// eps2023.github.io/)
[44] Michael C.A. *et al* 2023 *49th EPS Conf. on Plasma Physics* (*Bordeaux, France, July 2023*) (available at: https:// eps2023.github.io/)
[45] Helander P. *et al* 2002 *Phys. Rev. Lett.* **89** 235002
[46] Parr E. *et al* 2024 *Rev. Sci. Instrum.* **95** 013508
[47] Prechel G. *et al* 2023 *65th APS Division of Plasma Physics* (available at: https://meetings.aps.org/Meeting/DPP23/ Session/NP11.76)
[48] García-Muñoz M. *et al* 2010 *Phys. Rev. Lett.* **104** 185002
[49] Sanchis L. *et al* 2019 *Plasma Phys. Control. Fusion* **61** 014038
[50] Galdon-Quiroga J. *et al* 2022 *Nucl. Fusion* **62** 096004
[51] Zeeland M.V. *et al* 2015 *Nucl. Fusion* **55** 073028
[52] Kim K. *et al* 2018 *Phys. Plasmas* **25** 122511
[53] McClements K.G. *et al* 2015 *Plasma Phys. Control. Fusion* **57** 075003
[54] Sanchis L. *et al* 2021 *Nucl. Fusion* **61** 046006
[55] Bortolon A. *et al* 2013 *Phys. Rev. Lett.* **110** 265008
[56] Gonzalez-Martin J. *et al* 2023 *Phys. Rev. Lett.* **130** 035101
[57] (Available at: https://step.ukaea.uk/)